RSC Advances

ROYAL SOCIETY OF CHEMISTRY

www.rsc.org/advances

Controllable Synthesis of Uniform $CaMoO_4:Eu^{3+}$, M^+（M =Li，Na，K）Microspheres and Optimum Luminescence Properties

Xiaoguang Liu[1, 2, 3], Ling Li[1, 2], Hyeon Mi Noh [2], Jung Hyun Jeong [*2], Kiwan Jang[3], Dong Soo Shin[3]**

[1]Hubei Collaborative Innovation Center for Advanced Organochemical Materials, Ministry-of-Education Key Laboratory for the Synthesis and Applications of Organic Functional Molecules, Hubei University, Wuhan 430062, China

[2]Department of Physics, Pukyong National University, Busan 608-737, Korea

[3]Department of physics, Changwon National University, Changwon, Korea 641-773

*Corresponding author:

+82-51-629-6285; fax +82-51-629-5549(**Jung Hyun Jeong)**

+82-055-213-3427; Fax: +82-55-213-0263(**Kiwan Jang)**

E-mail addresses:

liuxiaoguang402@hotmail.com (Xiaoguang Liu);

liling402431@hotmail.com (Ling Li);

bwgn@naver.con (Hyeon Mi Noh);

jhjeong@pknu.ac.kr (J. H. Jeong);

kwjang@changwon.ac.kr (Kiwan Jang)

dsshin@changwon.ac.kr(Dong Soo Shin)

Abstract

High-quality and monodisperse $CaMoO_4:Eu^{3+}$, M^+ (M =Li, Na, K) microspheres have been synthesized with the assistance of poly-(diallyldimethylammonium chloride) (PDDA) via a facile coprecipitation hydrothermal route. X-Ray diffraction (XRD), scanning electron microscopy (SEM), energy dispersive X-ray spectrum (EDS), transmission electron microscopy (TEM), thermogravimetric analysis (TGA), X-ray photoelectron spectra (XPS), as well as photoluminescence (PL) spectra are used to characterize the resulting samples. The results show that the $CaMoO_4:Eu^{3+}$, M^+ (M =Li, Na, K) can be directly indexed to tetragonal $CaMoO_4$ phase with high purity. A series of controlled experiments indicate that PDDA as a shape modifier introduced into the reaction system plays a critical role in the morphology of the final products. Furthermore, the shape and size of the products can be further manipulated by adjusting the concentration of PDDA and pH values in the initial solution. The prepared microspheres are stable at a suitable annealing temperature. The possible formation mechanism for these microspheres is presented. Additionally, the PL properties of $CaMoO_4:Eu^{3+}$, M^+ (M =Li, Na, K) were investigated in detail. The results reveal that the red emission peak intensity of $CaMoO_4:Eu^{3+}$, Li^+ and $CaMoO_4$: Eu^{3+}, Na^+ is higher than that of $CaMoO_4:Eu^{3+}$, K^+. The particle size and shape have a remarkable effect on the photoluminescence properties of the phosphor. The luminescence intensity is observably enhanced with increasing of the annealing temperature due to eliminating PDDA and/or H_2O present in the samples and to the improved crystal quality.

1. Introduction

In recent years, the precise architectural manipulation of inorganic

nanocrystals, submicrocrystals and microcrystals with well-defined morphologies, excellent uniformity and monodispersity as well as accurately tunable sizes remains a research focus due to the close interrelation between the chemical and physical properties of materials and their geometrical factors such as shape, dimensionality, size and surface.[1, 2] Mastery over the shape, dimensionality and size of micro/nanocrystals not only enables control of its properties but also enhances their usefulness for a given application.[3, 4] Lanthanide-doped luminescent micro/nanomaterials exhibit interesting optical characteristics, which are poised to be exploited in the development of displays and phosphor applications[5].

Among various rare earth doped phosphors, molybdates with scheelite-like structures are widely used as hosts for the luminescence of rare-earth ions.[6] Metal molybdates ($AMoO_4$, A = Ca, Sr, Ba, Pb and Cd) have novel properties and great potential applications in various fields such as PL, catalysis, scintillator materials, magnetic properties, and microwave applications.[7-10] Among these materials, $CaMoO_4$ has been extensively studied due to its attractive luminescence behavior and interesting structural properties. Calcium molybdate ($CaMoO_4$) crystal, belonging to the scheelite type tetragonal structure is composed of deltahedral [CaO8] clusters and tetrahedral [MoO4] clusters with its space group $I41/a(C4h^6)$.[9] $CaMoO_4$ is attractive for the following reasons. First, $CaMoO_4$ is a highly transparent material which allows a wide range of light to pass through without much attenuation in luminescence. Second, $CaMoO_4$ is a robust phosphor due to its high density (4.25 g cm^{-3}) and possess better physical and chemical properties compared to other oxide materials. $CaMoO_4$ compounds are potentially attractive as phosphor materials for advanced lighting and display applications when doped with rare-earth ions.[11-15]

Recently, Eu^{3+}-doped $CaMoO_4$ in particular has been investigated

extensively as a red-emitting phosphor and was considered as ideal substitution for commercial red phosphors for WLEDs[16-19]. Furthermore, a few efforts have been devoted to improve luminescence efficiency of $CaMoO_4:Eu^{3+}$ for better performance[12, 14, 20, 21]. It is widely reported in literatures that the presence of alkali metal ions like Li^+, Na^+, and K^+ in $CaMoO_4$ matrix enhances the luminescence of Eu^{3+} ions significantly[21-23].

Many methodologies[16, 18, 19, 24-35] including conventional solid-state reactions, combustion methods, sol-gel, coprecipitation and hydrothermal method have been extensively studied to prepare $CaMoO_4$-based Micro/Nanocrystals that although attractive, still face issues in efficient control over the crystal size, morphology, and compositions that are crucial for high luminescence performance.

At present $CaMoO_4:Eu^{3+},M^+$ red phosphors micro/nanomaterials including aggregates sphere-like particles, octahedrons, nanosheets and nanowhiskers, hollow microspherical $CaMoO_4:Eu^{3+},Li^+$, $CaMoO_4:Eu^{3+},Na^+$ nanoparticles, three dimensional flake-ball and flake-disk $CaMoO_4:Eu^{3+},Na^+$superstructures have been successfully fabricated by different methods, such as a microwave-assisted solid-state reaction[36], molten salt synthesis[37], spray pyrolysis method[38], solvothermal method[39] and hydrothermal method[40]. For practical applications, the phosphors with spherical shape are highly needed over other morphologies due to that a) spheres can minimize the light scattering and b) a denser luminescence layer could be developed by high packing densities[41, 42]. Thus, it is still one of the most challenging issues for us to establish an efficient method to synthesize $CaMoO_4:Eu^{3+}$, M^+ red phosphors with an ideally spherical shape, a narrow size distribution, and highly dispersibility.

Solution chemistry via coprecipitation hydrothermal routes is advantageous for homogeneous nucleation of Micro/Nanocrystals with defined morphologies. Nevertheless, the nucleation rate is highly sensitive to the

supersaturation with respect to the relative activity of Ca^{2+}, and MoO_4^{2-}. As a result, it is still an outstanding problem as to the simultaneous substitution of Eu^{3+} and monovalent alkali metal ions at Ca^{2+} sites of $CaMoO_4$ when using solution chemistry. Having these in mind, regulation of the relative activity of reactive species (Ca^{2+}, MoO_4^{2}) by carefully choosing certain types of capping reagents such as PDDA is fundamentally. Important, which may help to simultaneously substitute Eu^{3+} and alkali metal ions at Ca^{2+} sites of $CaMoO_4$ for significantly improved luminescence intensity. Furthermore, negatively charged polyelectrolyte are widely used as an effective means to control the crystallization of inorganic materials[43-45], positively charged polyelectrolyte are generally considered to be much less active. The cationic polyelectrolyte Poly (diallyldimethyl-ammonium chloride) has recently been shown to exert significant control over $CaWO_4$ precipitation, driving the formation of shuttle-like nanostructures.[46] However, to the best of our knowledge, synthesis of monodisperse rare earth ions-doped $CaMoO_4$ microspheres and control of sizes have never been reported in any articles.

In this paper, poly-(diallyldimethylammonium chloride) (PDDA), as an environmentally friendly and low cost cationic polyelectrolyte, has been used as an effective means to control $CaMoO_4:Eu^{3+}$, M^+（M =Li，Na，K）precipitation. We prepared uniform and monodisperse $CaMoO_4:Eu^{3+}$, M^+（M =Li，Na，K）microspheres with controllable sizes through a facile and mass production coprecipitation hydrothermal route. The effects of the amount of PDDA, pH value of the initial solution, the molybdenum source, hydrothermal temperature and annealing temperatures on the phase compositions, morphologies, and luminescence properties have been investigated in detail. In addition, the possible formation mechanism of the microspheres is proposed. By using the method in this work, we show how one may control the chemical compositions and particle sizes of $CaMoO_4$-based red phosphors. The

simultaneous substitutions of Eu^{3+} and Na^{+} at Ca^{2+} sites are also demonstrated. This work provides some insight into the design of other well-defined molybdate functional materials.

2. Experimental Section

2.1 Materials

All chemicals were analytical grade and used directly without any further purification. $Eu(NO_3)_3.5H_2O$ were purchased from Shanghai Energy Chemical Limited Corporation (China). $Na_2MoO_4.2H_2O$, Li_2MoO_4, K_2MoO_4, $Ca(NO_3)_2.4H_2O$, nitric acid and Poly (diallyldimethyl-ammonium chloride) (PDDA, 20%, w/w in water) with average molecular weights of 200000–350 000 g/mol were purchased from Sigma-Aldrich Co. Deionized water was used throughout the experiment.

2.2 Preparation

In a typical synthesis procedure, 3.6 mL Ca $(NO_3)_2$ (0.5 mol /L), 4 ml Eu $(NO_3)_3$ (0.05 mol /L) were added into 17.4ml aqueous solution containing a certain concentration of Poly (diallyldimethyl-ammonium chloride) under magnetic stirring. After vigorous stirring for 20min, 25mL of aqueous solution containing 2 mmol $Na_2MoO_4.2H_2O$ was added drop wise into above solution. Then the pH value was adjusted to a given value by diluted NaOH solution or diluted HNO_3 and stirred for another 30 min. After that, the as obtained mixed solution was sealed in a 70 mL Teflon-lined stainless steel autoclave and heated to the required temperature for 12 h. Finally, when the autoclave was cooled to ambient temperature naturally, the white precipitates were separated by centrifugation, washed with deionized water and ethanol several times, and air-dried at 70℃for 10 h. For the preparation of Li^{+} or K^{+} charge compensated $CaMoO_4:Eu^{3+}$sample, the corresponding amounts of Li_2MoO_4 or K_2MoO_4were added to replace $Na_2MoO_4.2H_2O$ at the initial stage. As-prepared samples were annealed at 600°C, 700°C and 900 °C in air for 6 h with a heating rate of

2 °C·min^{-1}.

2.3 Characterization

The phase structure and purity of the prepared products were characterized by X-ray diffraction (XRD) patterns using a Rigaku UItima IV multipurpose X-ray diffraction system with Cu Kα (λ = 1.5405 Å) radiation at 40 kV and 30 mA. Field emission scanning electron microscopy (FE-SEM) images and energy-dispersive spectroscopy (EDS) were taken on a TESCAN VEGA II LSU scanning electron microscope. Transmission electron microscopy (TEM) observations and selected area electronic diffraction (SAED) patterns were performed on a JEOL JEM 2010 transmission electron microscope (TEM), using an accelerating voltage of 200 kV. The X-ray photoelectron spectra (XPS) were taken on a VG ESCALAB 2000 electron energy spectrometer using Al Ká(1486.6 eV) as the X-ray excitation source. Thermogravimetric analysis (TGA) was carried out on a TGA-60H thermal analyzer (Shimadzu Corporation) with the heating rate of 10 ℃min^{-1} in an air flow of 100 mLmin^{-1}. The photoluminescence (PL) and photoluminescence excitation (PLE) spectra were recorded by using a time-resolved Photon Technology International (PTI) fluorimeter with a Xe-arc lamp of power 60 W as the excitation source. The luminescent dynamic decay curves of Eu^{3+} were measured by using a phosphorimeter attachment to the main system (PTI) with a Xe-flash lamp (25 W) as the excitation source. All measurements were performed at room temperature.

3. Results and discussion

3.1 Phase, structure and morphology

During the formation process, PDDA plays a critical role in controlling the morphology and size of the final products. To investigate the effect of PDDA concentration on morphology and size evolution, a series of experiments were carried out using different PDDA concentrations, while other parameters were

kept identical. Firstly, the phase purity of as-synthesized samples using $Na_2MoO_4.2H_2O$ as a molybdenum source in the presence of PDDA were investigated by X-ray diffraction (XRD) patterns. The XRD patterns of as-prepared samples are exhibited in Figure1 (a)-(e). It can be observed from the XRD patterns that all the diffraction peaks are indexed as a pure tetragonal phase structure with a space group of I41/a ($C4h^6$), according to the standard data JCPDS card No. 29-0351. No discernible impurity or other phases can be detected, indicating that the prepared samples are high phase purity and the addition of PDDA and the doped Eu^{3+} ions has no influence on the phase transition of $CaMoO_4$. The strong and sharp diffraction peaks suggest that the synthesized samples are highly crystallized.

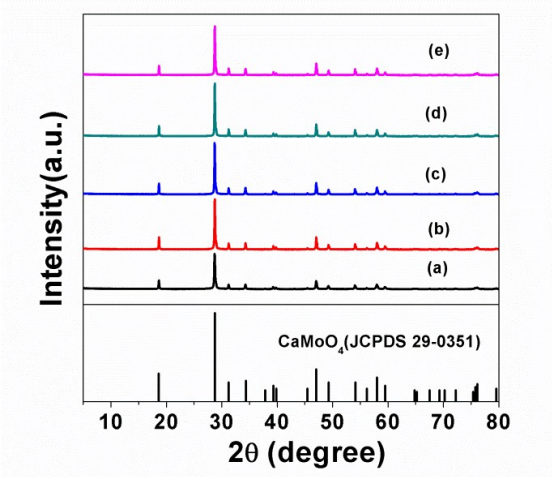

Figure 1. XRD patterns of prepared samples using $Na_2MoO_4.2H_2O$ as the molybdenum source at 100℃ for 12 h with different PDDA concentration while the Eu^{3+} doped concentration and pH were fixed at 10 mol% and 6.0 respectively. PDDA concentration: (a) 0 g /50ml, (b) 0. 1 g/50ml, (c) 0.2 g/50ml, (d) 1.0 g/50ml, (e) 2.0 g/50ml.

Figure 2 shows the SEM images and particle size distribution of as-prepared

samples with different PDDA concentrations. As seen from the SEM images, when no PDDA is added, only irregular particles are produced (Figure 2A, B). When the amount of PDDA is small (0.1 g/50ml), most of the irregular shaped particles disappear and a large amount of spherical-shaped particles aggregates are obtained (Figure 2C, D).These indicate that a small amount of PDDA already influences the morphology of the final products. Increasing the PDDA concentration to 0.2 g/50ml, more PDDA polyelectrolyte chain can be adsorbed on the surface of resulting particles. Furthermore, the selective adsorption leads to reduced surface energy and interfacial tension of formed particles. Consequently, surface agglomeration can be effectively hindered and large scale highly dispersibility uniform microspheres are obtained (Figure 2E, F). Figure 2 also shows that the diameter of the microspheres increases with farther increasing PDDA concentration. When the PDDA concentration increases from 0.2g/50ml, 1 g/50 ml to 2g/50 ml, the average diameter of the microspheres increases from 0.95μm (Figure 2E，F，K), 1.4 μm (Figure 2G, H，L), to 2.2μm (Figure 2I, J， M). The above results demonstrate that the size distribution of the microspheres can be controlled by choosing suitable PDDA concentration.

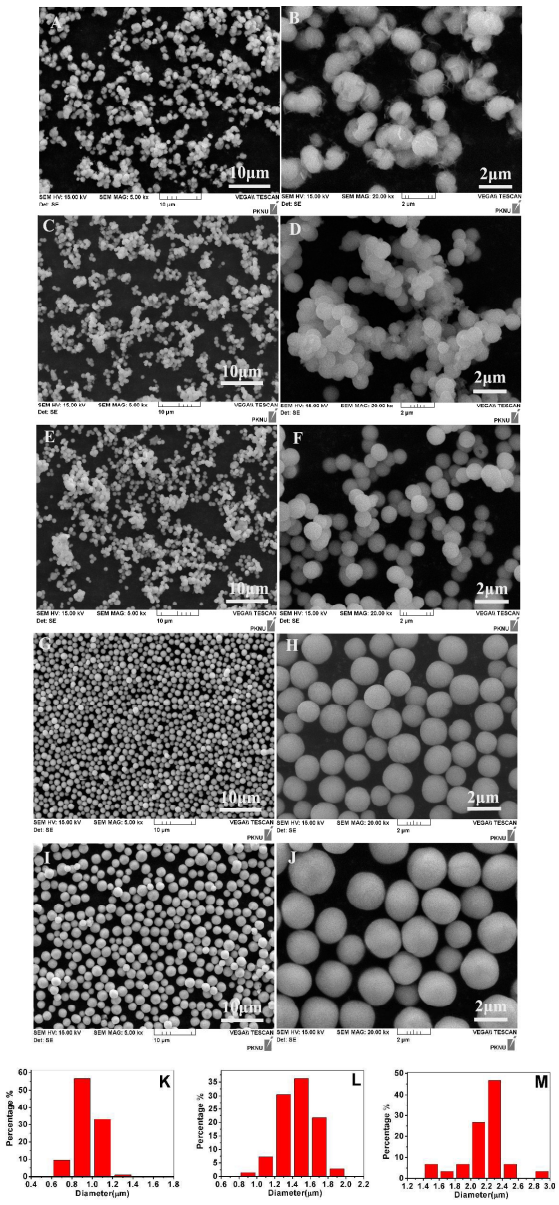

Figure 2. SEM images of prepared samples using $Na_2MoO_4.2H_2O$ as the molybdenum source at 100℃ for 12 h with different PDDA concentration while the Eu^{3+} doped concentration and pH were fixed at 10 mol % and 6.0 respectively. PDDA concentration: 0 g /50ml (A, B), 0. 1 g/50ml(C, D), 0.2 g/50ml (E, F), 1.0 g/50ml (G, H), 2.0 g/50ml (I, J). Distribution of particle size at different PDDA concentration: (K) 0.2 g/50ml, (L) 1.0 g/50ml, (M) 2.0 g/50ml.

Herein, we employ a cationic polyelectrolyte, poly-(diallydimethlammonium chloride) (PDDA) includes hydrophilic groups (positively charged quaternary ammonium groups parts) and hydrophobic groups (hydrocarbyl parts) as the capping agent and stabilizer simultaneously in a facile synthesis process. PDDA acts as a stabilizer experiencing steric repulsion and electrostatic stabilization with the attachment of neighboring PDDA molecules. The assembling process of microspheres reduces the overall energy by minimizing the surface energy. Notably, a sufficient amount of PDDA is necessary to control the crystal growth process and achieve the final microspheres.

On the basis of these results, when the PDDA concentration is high, positively charged hydrophilic groups move outward spontaneously to form a spherical-like micelle structure with large amounts of amino groups exposed. Furthermore, PDDA induces the rate of nucleation $CaMoO_4:Eu^{3+}$, Na^+, which is attributed to phase separation based on the electrostatic interaction between the quaternary ammonium groups on the PDDA and the negatively charged molybdate ions. At much higher PDDA concentration, the nucleation of $CaMoO_4:Eu^{3+}$, Na^+ easily occurs in the chemical microenvironments near the region of the PDDA chains. And therefore, the induction time of precipitation decreases and fewer $CaMoO_4:Eu^{3+}$, Na^+ particles are formed. It is not surprising that the particle sizes increase slightly with increasing of the PDDA concentration. The above results powerfully demonstrate that the PDDA concentration plays a crucial role in determining the size and morphology of the products.

In this work, the products achieved at the concentration of PDDA 1.0 g/50ml were selected as the representative samples and TEM, SAED, EDS, XPS and TGA were used to further investigate the detailed morphological, composition and structure features of the products.

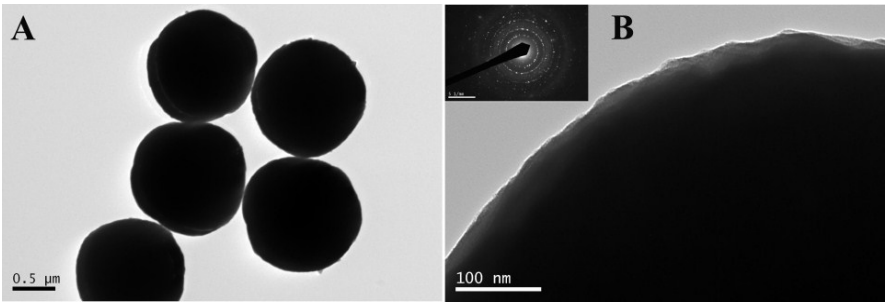

Figure 3. (A) Low-magnification and (B) high-magnification TEM images of the as-prepared microspheres at the concentration of PDDA 1.0 g/50ml. The inset of (B) is the corresponding SAED pattern.

The detailed morphology of the as prepared microspheres was further examined by TEM. The TEM images of the prepared samples with 1.0g/50ml PDDA concentration were shown in Figure 3, from which we can clearly see that the particles are uniform in size, highly dispersibility, with an ideally spherical shape. This is well consistent with the corresponding SEM images (Figure 2 G, H). Close observation of the high-magnification TEM image in Figure 3B reveals that the microspheres have clear edges and smooth surfaces with a solid interior. The corresponding selected area electron diffraction (SAED) pattern (inset of Figure 3B) of individual particles exhibits the well-defined, crystalline structure, which is in good agreement with the XRD result (Figure 1d).

It is well-known that $CaMoO_4$ crystallizes into a tetragonal scheelite structure with space group *C*4*h*, in which Ca^{2+} is coordinated with eight oxygen atoms and has a S4 point symmetry with no inversion center.[47] These considerations led us to assume that Eu^{3+} may be doped into the Ca^{2+} sites of the samples, in agreement with the ionic radii difference because the ionic radii of 0.947 Å for Eu^{3+} is slightly smaller than that of 1.00 Å for Ca^{2+},but much larger than that of 0.59 Å for Mo^{6+}in 4-fold coordination. Nevertheless, the difference

in oxidation states between Eu^{3+} and Ca^{2+} would result in the deviation of the site symmetry of Eu^{3+} from S4 symmetry due to the charge compensation effects. Ghaderi and co-workers[48] proposed two types of charge compensating patterns, hump-shaped (type I) and flat (type II), for Eu^{3+} substitution in Ca^{2+} sites via the paths: $2\ Ca^{2+} = Eu^{3+} + Na^{+}$ for type I and $3Ca^{2+} = 2Eu^{3+} + \square$ (where $\square$ is a Ca site vacancy) for type II. Considering the proposal of Ghaderi et al..[48] This type of charge compensation pattern could exist in the present samples? To answer this question, it is necessary to measure samples composition.

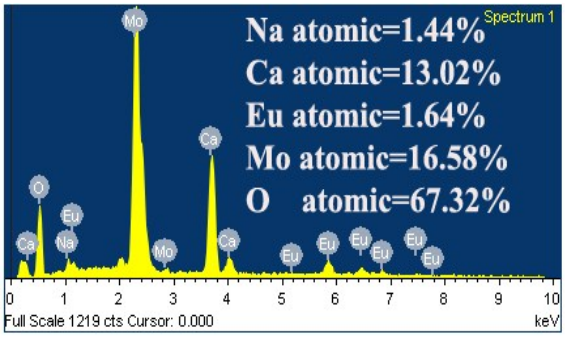

Figure 4. EDS spectra of as-prepared sample at the concentration of PDDA 1.0 g/50ml

Firstly, the Elemental dispersive spectrum (EDS) analysis was performed on as-prepared microspheres to identify the elements present and measure their composition. Figure 4 shows the EDS spectra of as synthesized microspheres with PDDA as the capping agent. The EDS result confirms the presence of Ca, O, Mo, Na and Eu elements in the samples. And also the concentration of Eu^{3+} in the samples was determined to be 9.9%, which is close to their feed ratios. The existence of Na^{+} in the samples is clear in their corresponding EDS spectra. The ratio of Na and Eu atomic number in the samples is about 0.88:1, suggesting formation of $CaMoO_4$:Eu^{3+}, Na^{+}. It is easy to see the effective incorporation of the Eu^{3+} and Na^{+} into the $CaMoO_4$ matrix.

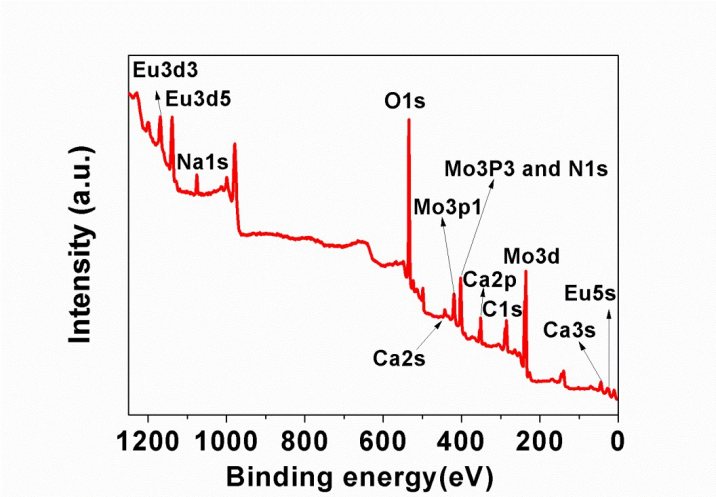

Figure 5. XPS spectrum of the $CaMoO_4:Eu^{3+}$, Na^+ microspheres at the concentration of PDDA 1.0 g/50ml

Further evidence for the chemical composition on the surface of the as-prepared $CaMoO_4:Eu^{3+}$, Na^+ microspheres was analyzed by the XPS technique. Figure 5 shows the XPS survey spectra of $CaMoO_4:Eu^{3+}$, Na^+ microspheres synthesized with PDDA. The XPS survey spectrum confirms the presence of Ca, Mo, O, Eu, Na, N and C elements in the synthesized samples surface. The C(1s, 285.21 eV) and N(1s,401.97) peak were assigned to the PDDA capped on the $CaMoO_4:Eu^{3+}$, Na^+ microspheres surface，which is due to the highest PDDA absorption during the synthesis. In addition, the binding energy of Na (1s, 1075.77 eV) can be clearly seen from the XPS survey spectrum, suggesting the existence of Na in the microspheres.

Table 1: Surface Composition of the $CaMoO_4:Eu^{3+}$, Na^+ Microspheres Synthesized with PDDA Estimated through XPS Analysis

$CaMoO_4:Eu^{3+},Na^+$	O (1s)	Mo(3d)	Ca(2p)	Eu(3d5)	Na(1s)	C(1s)	N (1s)
Peak position (eV)	534.12	236.28	350.93	1139.14	1075.77	285.21	401.97

(atom%)	33.39	8.31	3.41	1.38	1.29	31.45	20.77

The surface compositions of the $CaMoO_4:Eu^{3+}$, Na^+ particle synthesized using PDDA as a capping agent Estimated through XPS analysis were shown in Table1. According to the data represented in Table 1 we observe that the atomic ratio of Na: Eu is estimated to be 0.93, which is close to EDS result. By combination of EDS and XPS results, it can be deduced that alkali metals ions Na^+ are added into the host as the charge compensation agent. In our present work, we demonstrate the feasibility of intentionally introducing alkali ions (M^+) into the vicinity of Eu^{3+}. Once a Ca^{2+} site is substituted for a Eu^{3+} ion, an alkali ion M^+ would preferentially locate in the neighborhood of Eu^{3+} as a result of charge compensation. In this way, the microenviroment around Eu^{3+} can be modified by the introduction of different types of alkali metals ions like Li^+, Na^+, and K^+.

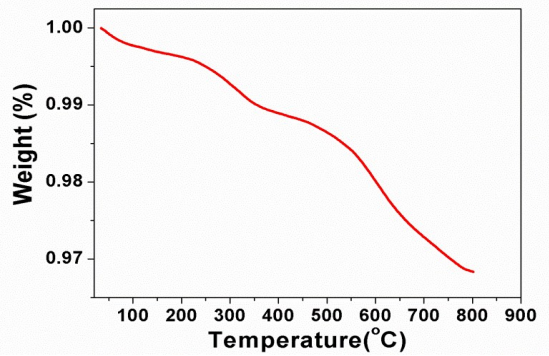

Figure 6. TGA curve of $CaMoO_4$: Eu^{3+}, Na^+ microspheres at the concentration of PDDA 1.0 g/50ml

The thermal behavior of $CaMoO_4$: Eu^{3+}, Na^+ microspheres was analyzed by TG technique (Figure 6). The result shows that the $CaMoO_4:Eu^{3+}$, Na^+ microspheres contained PDDA and little water. The mass loss between 200 and 800 ℃ is ascribed to the decomposition and desorption of residual PDDA. The

amount of PDDA in the microspheres is about 2.8 wt %. These results indeed show that limited amount of PDDA molecules are incorporated into the microspheres

3.2 Influence of factors on the Phase identification and morphology

Influence of pH values

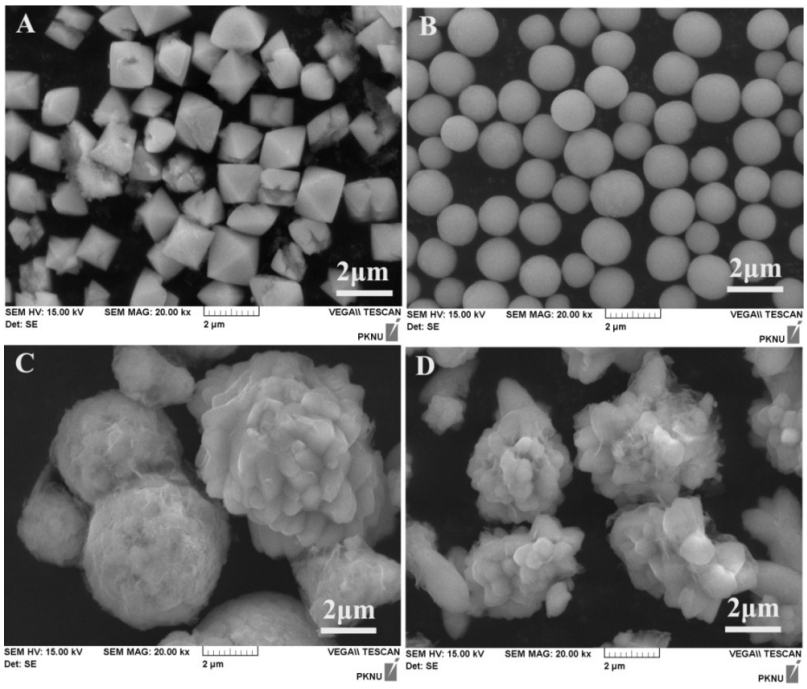

Figure 7. SEM images of $CaMoO_4$: Eu^{3+}, Na^+ prepared with different pH values of 4.0 (A), 6.0 (B), 7.0 (C), 10.0 (D).

The variation of pH obviously influences the morphology of the as-obtained $CaMoO_4$:Eu^{3+}, Na^+ products. Figure 7 shows the SEM images of the products obtained under the same conditions but at various pH values. The corresponding XRD patterns were shown in Figure 8. As seen from the SEM images, $CaMoO_4$: Eu^{3+}, Na^+ materials with various morphologies can be obtained by simply adjusting the pH values of the suspension solution. At pH = 4, the obtained

$CaMoO_4:Eu^{3+}$, Na^+ products exhibit octahedral-shaped morphology and smooth surfaces (Figure 7A). On increasing the pH value to 6, morphology of the products greatly varies. It can be clearly seen from Figure 7B, that there are a large quantity of highly dispersibility uniform $CaMoO_4:Eu^{3+}$, Na^+ microspheres with an average diameter of about 1.4 μm. When the pH value is varied from 6 to 7 (Figure 8c), uniform microspheres disappear and two kinds of morphologies of the product coexist: nonregular large spheres particles and flower-like architectures composed of small particles irregular aggregates on the surface of the product, but they share the same XRD pattern (Figure 8). When the pH is further increased to 10, the morphology of the corresponding product is basically maintained flower-like architectures (figure 7D).

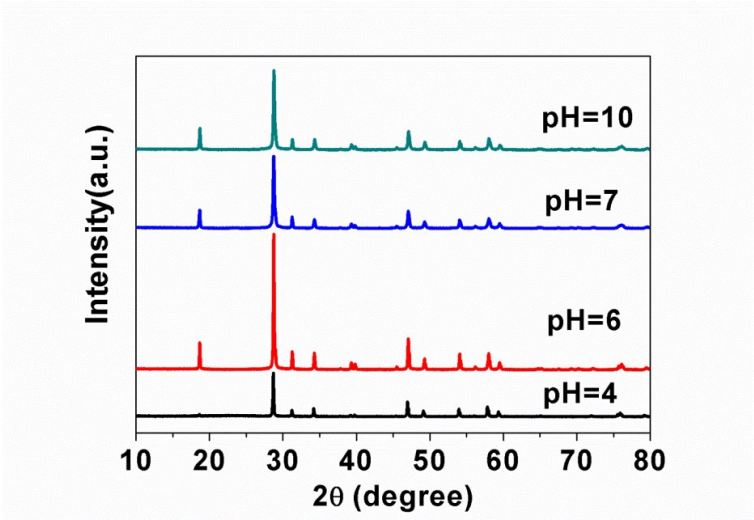

Figure 8. XRD patterns of $CaMoO_4:Eu^{3+}$, Na^+ prepared with different pH values of 4.0 (A), 6.0 (B), 7.0 (C), 10.0 (D).

On the basis of the experimental results, it is clear that the morphology of the final product strongly depended on the pH of the initial solution in our case. The pH is critical for directing the intrinsic shapes of the crystals due to its characteristic symmetry and structure, and change the growth rate of crystallographic planes with different surface energies so as to form different

crystallite morphologies[27, 49-51]. Otherwise, the pH may affect the intensity of the electrostatic attraction between PDDA and crystal facets.[52, 53] As the pH increased, $CaMoO_4:Eu^{3+}$, Na^+ nucleating process occurs faster and more nuclei are formed and large numbers of $CaMoO_4:Eu^{3+}$, Na^+ nuclei tend to aggregate together to form larger irregular particles during the reaction process. Therefore, pH value of 6 is optimal for good crystallization.

Influence of hydrothermal temperature

In order to improve luminescence performance of $CaMoO_4:Eu^{3+}$, Na^+ phosphor, the subsequent hydrothermal treatment is necessary. The effect hydrothermal temperatures on the morphology of the final products were shown in the Figure 9. As seen from the SEM images, when the hydrothermal temperatures is not more than 140 °C, the morphology of the final products does not show obviously change. As the hydrothermal temperature reach 180 °C, the surface of microspheres is coarse, this is ascribed to the decomposition and desorption of the PDDA in the surface of microspheres.

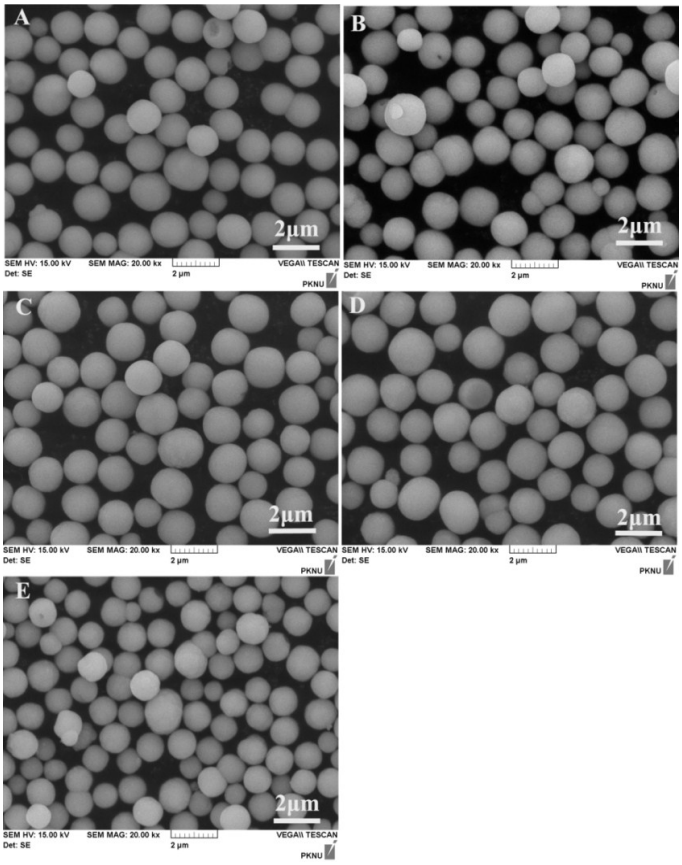

Figure 9. SEM images of $CaMoO_4:Eu^{3+}$, Na^+ prepared with different hydrothermal temperature 20°C (A), 80°C (B), 100°C (C), 140°C (D), 180 °C (E).

Influence of annealing temperature

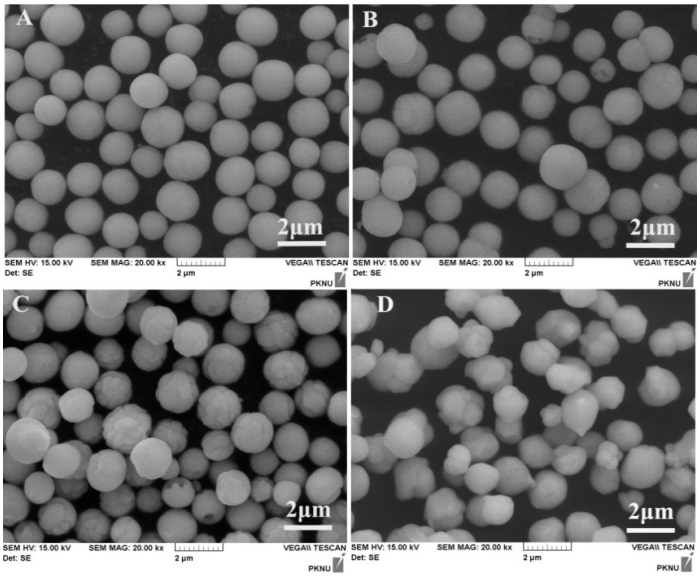

Figure 10. SEM images of $CaMoO_4:Eu^{3+}$, Na^+ annealed at different temperatures: as-prepared (A), 600°C (B), 700°C (C), 900°C (D).

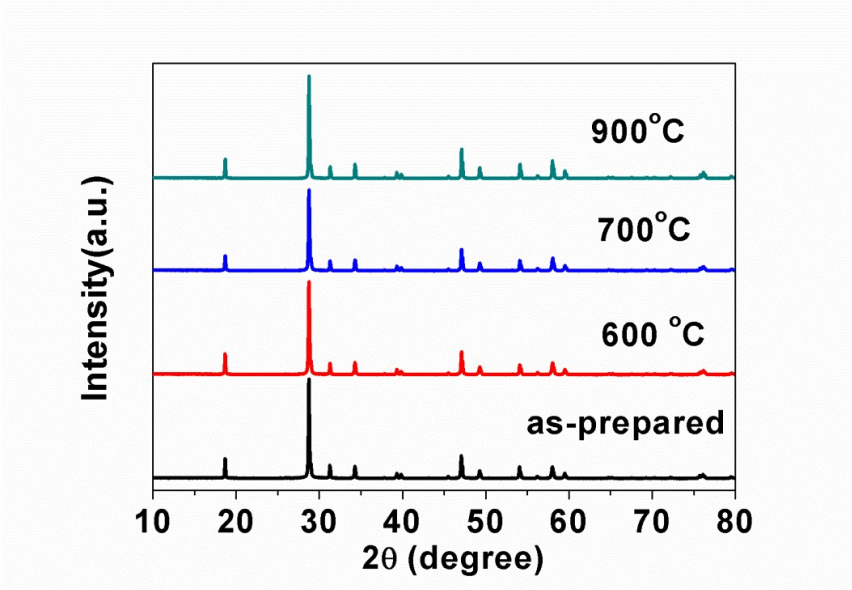

Figure 11. XRD patterns of $CaMoO_4$: Eu^{3+}, Na^+ as-prepared, 600°C, 700°C and 900 °C annealed.

To remove PDDA and/or H_2O present in the samples and determine the effect of the annealing temperature on the $CaMoO_4:Eu^{3+}$, Na^+ microspheres

morphology, as-prepared samples were annealed for 6 h at three different temperatures, 600, 700 and 900℃. The SEM images of samples annealed at different temperatures were shown in the Figure 10. It can be seen from Figure 10, $CaMoO_4:Eu^{3+}$, Na^+ still retains the microspheres morphology, except for a little bulge as the exterior of the microspheres because of the gradual elimination of organic elements at 700℃ annealing temperature. When the annealing temperature is further increased to 900℃, $CaMoO_4:Eu^{3+}$, Na^+ particles morphology is changed from spheres to irregular shaped particles.

The XRD patterns of $CaMoO_4$: Eu^{3+}, Na^+ at different annealing temperatures were also shown in Figure 11. Based on the XRD results, the calculated crystallite sizes for as-prepared, 600, 700 and 900 ℃ are 105, 98, 96.5 and 158.6 nm, respectively. The annealing process can be divided into two stages, namely remove PDDA and Ostwald ripening. When the annealing temperature is not more than 700℃, the PDDA gradually ashing and can be removed. The procedures are mainly provided for removing PDDA. The average size of the grains has seldom changed as a consequence of annealing temperature. Therefore the morphological of $CaMoO_4:Eu^{3+}$, Na^+ microspheres are obviously independent of the annealing temperature. When the annealing temperature increases from 700 to 900℃, The average size of the grains increase obviously with the increase of the annealing temperature as a consequence of Ostwald ripening.[54] This result indicates that the crystal quality of the $CaMoO_4:Eu^{3+}$, Na^+ has changed little, and these microspheres morphology are stable when the annealing temperature is not more than 700℃. At higher annealing temperatures the crystal quality of the $CaMoO_4:Eu^{3+}$, Na^+ is significantly improved, however these microspheres morphology are unstable.

The effect of different alkali metals ions

According to above results, Eu^{3+} and Na^+ are able to incorporation into the

host $CaMoO_4$, when $Na_2MoO_4.2H_2O$ as the molybdenum source. These considerations led us to assume that alkali metals ions Li^+ and K^+ may be doped into the Ca^{2+} sites of the samples. For the preparation of Li^+ or K^+ charge compensated $CaMoO_4:Eu^{3+}$sample, the corresponding amounts of Li_2MoO_4 or K_2MoO_4were added to replace $Na_2MoO_4.2H_2O$ at the initial stage.

In our current system, X_2MoO_4(X =Li, Na, and K) was added, the only difference lies in the cations in the initial solution. In this way, the microenvironment around Eu^{3+} can be modified by the introduction of different types of alkali metals ions like Li^+ and K^+. The phase purity of as-synthesized samples using Li_2MoO_4 or K_2MoO_4 as a molybdenum source in the presence of PDDA were investigated by X-ray diffraction (XRD) patterns. The XRD patterns of as-prepared samples were exhibited in Figure12 (a)-(c). It can be observed from the XRD patterns that all the diffraction peaks are indexed as a pure tetragonal phase structure with a space group of I41/a ($C4h^6$), according to the standard data JCPDS card No. 29-0351. No discernible impurity or other phases can be detected, indicating that the prepared samples are high phase purity. The typical SEM images of the prepared products with different molybdenum source were shown in Figure 13A–F, respectively. By comparison with $Na_2MoO_4.2H_2O$ as the molybdenum source, it clearly shows that the products prepared using Li_2MoO_4 as the molybdenum source is composed of numerous uniform microspheres, with the diameter of 1.4μm. However, the products prepared using K_2MoO_4 as the molybdenum source is composed of inhomogeneous microspheres.

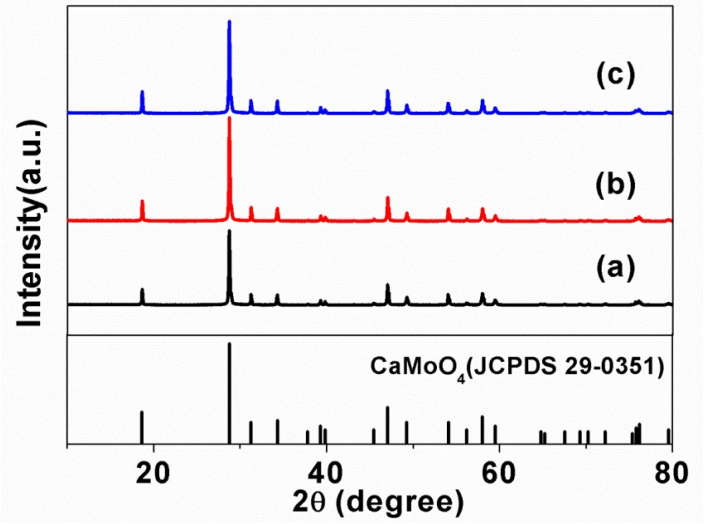

Figure 12. XRD patterns of prepared $CaMoO_4:Eu^{3+}$, M^+ using Li_2MoO4 (A), $Na_2MoO_4.2H_2O$ (B), and K_2MoO_4 (C) as the molybdenum source with a PDDA concentration of 1g/50ml at 100 ℃ for 12 h, respectively. Eu^{3+} doped concentration was 10 mol %，pH=6.0.

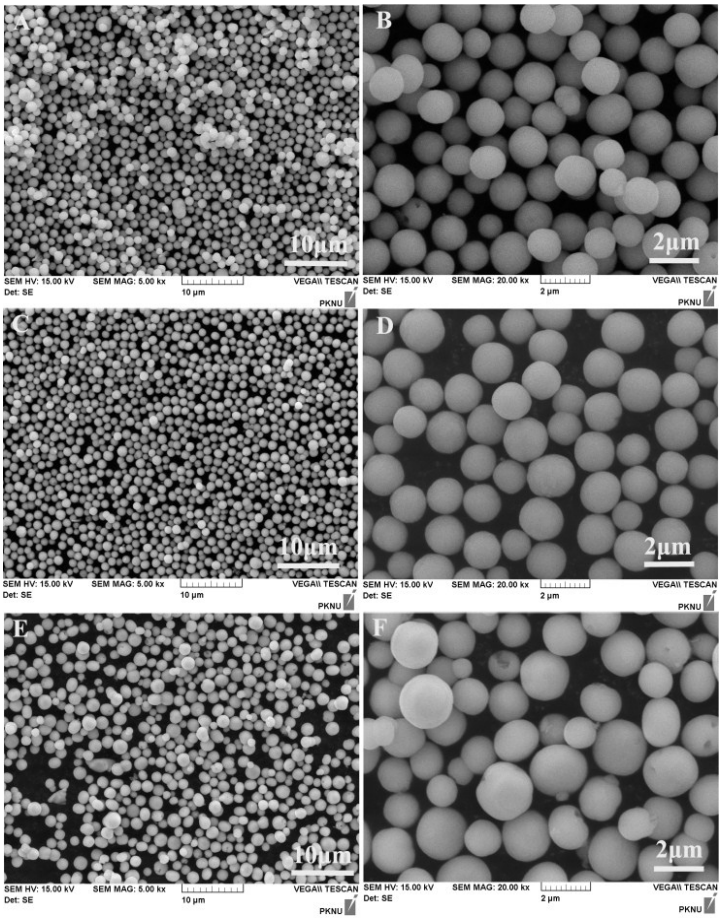

Figure 13. SEM images of the obtained sample by using Li_2MoO_4 (A, B), $Na_2MoO_4.2H_2O$ (C, D), and K_2MoO_4 (E, F) as the Mo source, respectively.

3.3 Possible formation mechanism $CaMoO_4:Eu^{3+}$, M^+（M =Li，Na，K）microspheres

On the basis of the above experiment results and the morphological evolution evidence, Figure 14 summarizes the possible formation processes of $CaMoO_4:Eu^{3+}$, M^+ (M =Li，Na，K) microspheres. The $CaMoO_4:Eu^{3+}$, M^+ microspheres formation process is considered as a three-step system: nucleation, aggregation and isotropic growth processes. First of all, the $CaMoO_4:Eu^{3+}$, M^+(M =Li，Na，K) formation for moderate supersaturation level, the nucleation process took place, and the amorphous $CaMoO_4:Eu^{3+}$, M^+(M =Li，

Na，K) elementary clusters[55-57] were formed as precursors in this step. In the subsequent process, the elementary clusters aggregated together to form metastable crystalline primary grains, and this led to the reduction in surface energy, and then the nearly uniform nanoparticles aggregated to form the highly monodisperse spheres. Simultaneously, the PDDA molecules evenly adsorb onto the surface of the particles in all directions to form a protective layer through electrostatic attraction, thus holding back the growth rate of the crystals and forming isotropic growth. After the spherical $CaMoO_4:Eu^{3+}$, M^+（M =Li，Na，K）microparticles underwent a recrystallization and ageing process. Due to the sufficient PDDA in the reaction system, the particles are well dispersed instead of being agglomerated. Consequently, the uniform monodisperse $CaMoO_4:Eu^{3+}$, Na^+ (Li^+) microspheres are obtained with smooth surface.

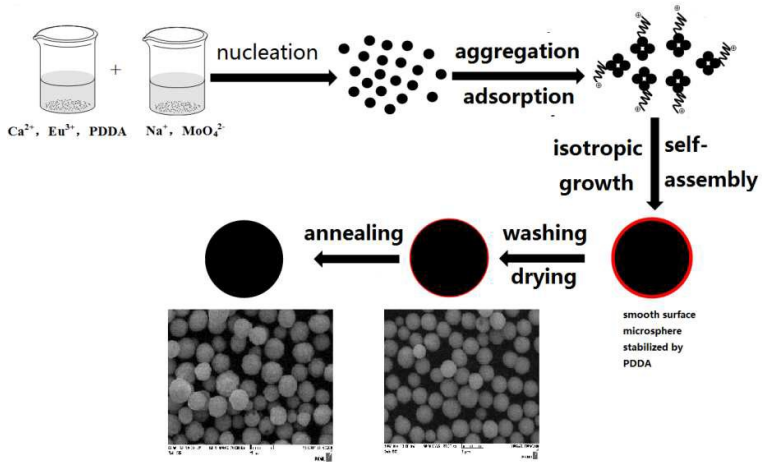

Figure 14. Schematic illustration of the possible formation process of $CaMoO_4:Eu^{3+,}$ M^+（M =Li，Na，K）microspheres

3.4 Luminescence properties

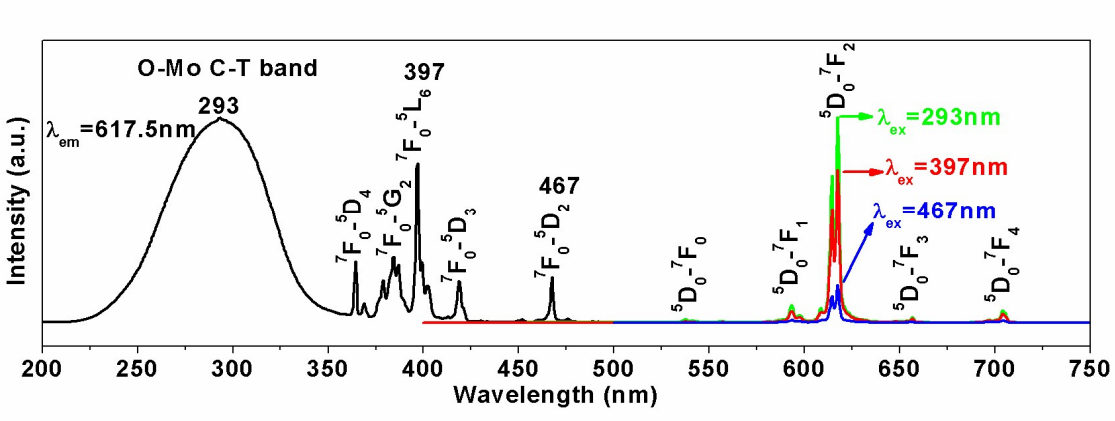

Figure 15. Excitation and emission spectra of $CaMoO_4:Eu^{3+,}$ Na^+ phosphors with the microspheres morphology

The photoluminescence properties of the as-prepared $CaMoO_4:Eu^{3+,}$ Na^+ phosphors were investigated in detail at room temperature. As shown in Figure 15, the excitation spectrum of the $CaMoO_4$: $Eu^{3+,}$ Na^+ samples consists of a wide absorption band from 200 to 350 nm centered at 293 nm and several sharp lines such as $^7F_0$-$^5L_6$ line at around 397nm and $^7F_0$-$^5D_2$ line at around 467 nm, which can be ascribed to the charge-transfer band between the O^{2-} and Mo^{6+} ions[58] and the f–f transitions within the $4f^6$ configuration of the Eu^{3+} ions, respectively. Upon excitation with UV (293 nm), near UV (397 nm) and blue (467 nm) wavelength light, the emission spectrum of $CaMoO_4:Eu^{3+,}$ Na^+ shows a typical Eu^{3+} red emission. These emission peaks are centered at 537, 593, 617.5 (614), 657, and 704 nm, which can be described as the well-known $^5D_0$–^7F_J (J = 0, 1, 2, 3, 4) radiative transition of the Eu^{3+} ions, as labeled in Figure 14, respectively. Obviously, the strongest emission peak is located at 617.5 nm, which is due to the typical forced electric dipole transition $^5D_0$–$^7F_2$ of the Eu^{3+} ions. As well-known to us, the intensities of different $^5D_0$–^7F_J transitions depend on the local symmetry of the crystal field of the Eu^{3+} ions. The $^5D_0$–$^7F_2$ transition is hypersensitive, while the $^5D_0$–$^7F_1$ transition is insensitive to the crystal field environment. For instance, in a site with an inversion symmetry, the magnetic

dipole transition is dominant, while in a site without inversion symmetry, the $^5D_0$–$^7F_2$ electronic transition becomes the strongest one.[59, 60] The intensity of $^5D_0$–$^7F_2$ transition is much higher than that of $^5D_0$–$^7F_1$, which is strong evidence that Eu^{3+} ions mainly occupy the lattice site without inversion symmetry.

It is well-known that $CaMoO_4$ crystallizes into a tetragonal scheelite structure with space group *C*4*h*, in which Ca^{2+} is coordinated with eight oxygen atoms and has S4 point symmetry. In our system, Eu^{3+} and Na^+ codoped in $CaMoO_4$ lattice would lead to a charge balance and moreover a reduction in Ca^{2+} vacancy concentration. Eu^{3+} and Na^+ codoped in $CaMoO_4$ matrix may induce a lattice distortion and lowered lattice symmetry. This assumption could be verified by the presence of the very weak $^5D_0$–$^7F_0$ emission at 537 nm in the emission spectra since the $^5D_0$–$^7F_0$ emission is only allowed for *Cs*, *Cn*, *Cn*υ site symmetry.[61]Furthermore, the codoped Eu^{3+} and Na^+ at Ca^{2+} sites in prepared samples also plays a very important role in the enhanced luminescence intensity. Numerous papers have reported that the addition of alkali metal ions into the rare-earth-doped materials results in a significant enhancement of the luminescence properties, which is all based on the modifications of the local symmetry and the surroundings near the rare earth ions by the addition of coactive ions or charge compensators of alkali metal ions.[22, 37, 62, 63] For the present work, when Na^+ ions are incorporated into $CaMoO_4$ lattice in/near Eu-O8 cluster to maintain a local charge balance between Eu^{3+} and Na^+, the structure of the Eu-O8 would not be destroyed but a slight structural modification and the resulting lowered symmetry of the crystal field around Eu^{3+}.

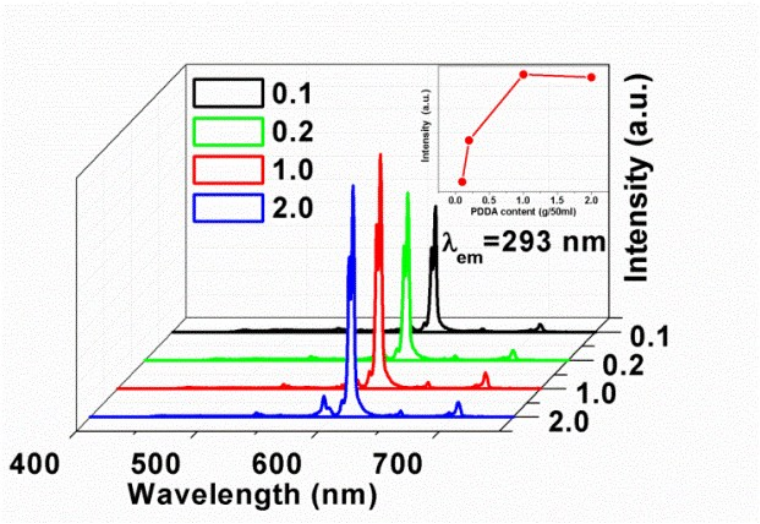

Figure 16. Emission spectra of $CaMoO_4:Eu^{3+}$, Na^+ at different PDDA concentration

In general, particle size and shape will affect the optical properties of phosphors. A series of experiments were carried out to explore the relationship between particle size, shape, and the fluorescent properties. Emission spectra of samples prepared with different PDDA concentrations ([PDDA]: 0.1 g /50ml, 0.2 g/50ml, 1 g/50ml and 2 g/50ml) were given in Figure 16. The differences in the particle sizes (Figure 2) will affect the scattering and absorption of incident light, so the emission intensities of the samples should be different. As shown in Figure 15, the luminescent intensity $CaMoO_4$: Eu^{3+}, Na^+ first observably enhance, and then very slight weaken with the increasing of the PDDA concentration. This is two reasons resulting. on the one hand, larger size particles have much stronger emission intensity than of smaller samples, because larger particles imply smaller surface area and less activator ions near to the surface to suffer from the surface-defect resulting in less nonradioactive decay losses of the surface luminescence ions. On the other hand, in our experiment, the PDDA is a water soluble polymer, the PDDA concentration increases, the particles size increases, and then larger size particles have much thicker adsorbed layer than of smaller

samples. On increasing the PDDA concentration to 2g/50ml, the luminescent intensity slight weaken. This is possibly due to a quenching effect from the surface PDDA or H_2O over the particles.

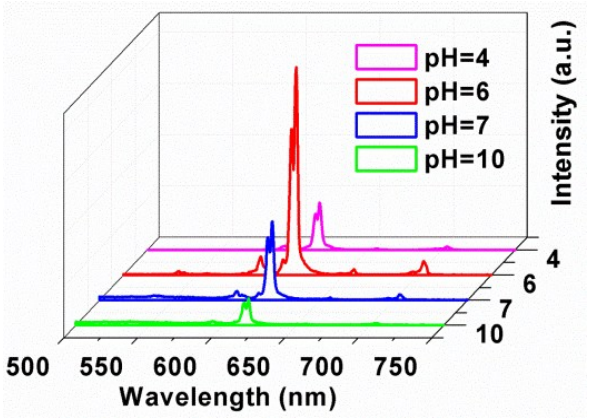

Figure 17. Emission spectra of $CaMoO_4:Eu^{3+}$, Na^+ at different pH value

It is commonly accepted that the PL properties of inorganic materials are strongly dependent on their sizes, morphologies, and crystallinity. From Figure 17, it can be clearly seen that the emission spectra of the products synthesized at different pH are similar in shape, but different in the intensity to some extent, indicating that the luminescent properties are closely correlated with the morphologies of the materials. Under identical measurement conditions, the sphere-shaped microstructure (red line) has the highest relative emission intensity, while the flower-shaped structures (green line) exhibit the lowest intensity. It is thus inferred that the morphology of the microsphere is more beneficial than the morphology of octahedral-shaped morphology and flower-like to the emission in the red region. The possible reasons for the difference of emission intensities can be deduced as follows. On the one hand, this interesting phenomenon might arise from the difference in the effects of crystal field perturbation on the in dividable f–f transition as a consequence of the different morphologies of the four samples. In our cases, the PL intensity of the sphere-

shaped microstructure is higher than that of the others samples. The enhanced luminescence performance due to microsphere has less surface defect than the other three samples. On the other hand, the electronic structures could be modified by means of the changes of the shapes of samples, which influences the excitation of the carriers from the valence band to the conduction band and the numbers of photons released from the surfaces of samples.[64] All of the aforementioned observations support the concept of morphology-dependent properties of $CaMoO_4:Eu^{3+}$, Na^+ samples and emphasizes the importance of morphology control.

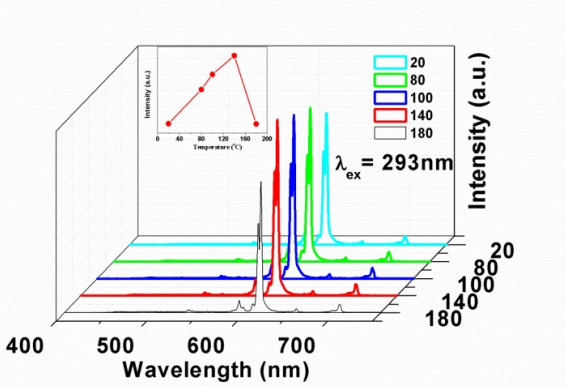

Figure18 Emission spectra of $CaMoO_4:Eu^{3+}$, Na^+ at different hydrothermal temperatures

Figure 18 showed the emission spectra of $CaMoO_4:Eu^{3+}$, Na^+ phosphors prepared at various temperatures between 20 and 180°C. From Figure 18, it can be seen that the emission intensity increases gradually with increases in the temperature up to 140°C, and then decreases dramatically at 180 °C, as shown in the inset in Figure 18. The $CaMoO_4:Eu^{3+}$, Na^+ prepared at 140°C is found to have the largest emission intensity. As is for the microcrystals prepared by wet chemical methods, the surfaces of the particles are covered by a great number of hydrophilic groups or H_2O either chemically bonded or physically adsorbed on the surfaces. These hydrophilic groups or H_2O can be the very efficient quenchers of the luminescence of lanthanide elements through multiphonon

relaxation.[65] Huignard and co-workers demonstrated that the transfer of YVO4:Eu^{3+} colloidal from water to deuterated water reduces the multiphonon relaxation and thus enhances the luminescent efficiency.[66] The sample prepared at room temperature has much more surface hydrophilic groups or H_2O than that obtained after hydrothermal treatments. As the hydrothermal treatment temperature reached 180 °C, the emission intensity decreases remarkably, this is ascribed to the decomposition of the PDDA in the surface of microspheres.

The photoluminescence properties of the $CaMoO_4:Eu^{3+,}$ Na^+ samples annealed at different annealing temperatures were investigated in detail at room temperature. Figure 19 showed excitation spectra and emission spectra of $CaMoO_4:Eu^{3+}$, Na^+ at different annealing temperatures. Generally, the excitation position and its full width at half maximum (FWHM) are affected by the environmental factor surrounding the centre ion Mo^{6+}, and the intensity of $^5D_0 \rightarrow {}^7F_2$ emission is sensitive to the distortion degree of EuO_8 polyhedron[58]. From Figure 19(a), it can be clearly seen that the excitation spectra of the products annealed at different temperatures are similar in shape and position by monitoring the emission wavelength at 617.5 nm. It indicates that the environmental factor surrounding the Mo^{6+} ions has no change at different temperatures. An emission trend was observed for the $CaMoO_4:Eu^{3+}$, Na^+ microspheres as a function of the annealing temperature, as shown in Figure 19 (b), emission intensity at 614 nm and 617.5 nm increases in the following order of annealing temperature as-prepared 600°C, 700°C, and 900 °C. The luminescence intensity is enhanced significantly by annealing at 600 °C than that of as-prepared sample. It indicates that the distortion degree of EuO_8 polyhedron is increasing with increasing of the annealing temperature. This may be attributed to eliminate of the PDDA by annealing resulting in decrease of the non-radiative transition probability. Up to 600 °C, there is almost no change in microspheres morphology (Figure 10). As compared to the as-prepared, 600 °C

and 700°C annealed samples, 900 °C annealed samples have high luminescence intensity. However, the peak positions are almost unaffected for 900 °C annealed samples. Improvement of luminescence is related to the extent of the improved crystal quality and decrease of non-radiative rate arising from the surface defect after annealing at higher temperatures.

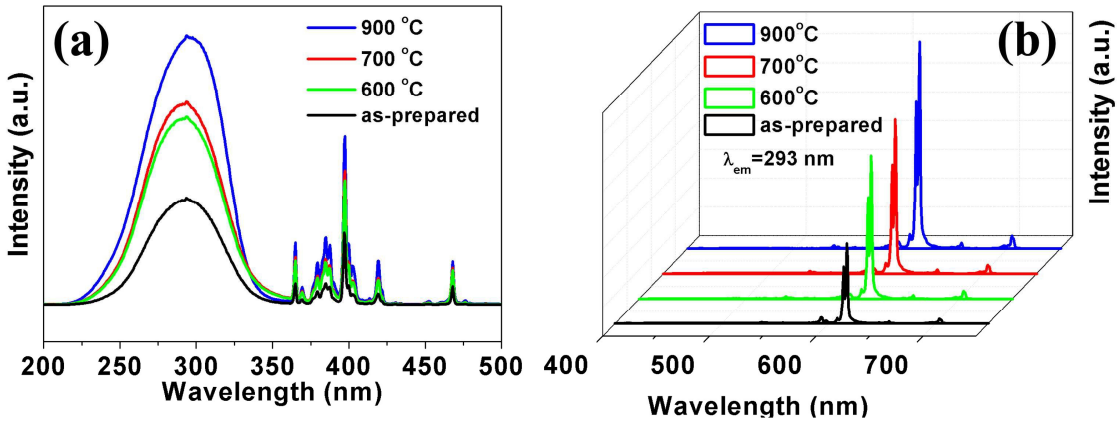

Figure 19. (a) Excitation and (b) Emission spectra of $CaMoO_4:Eu^{3+}$, Na^+ at different annealing temperatures.

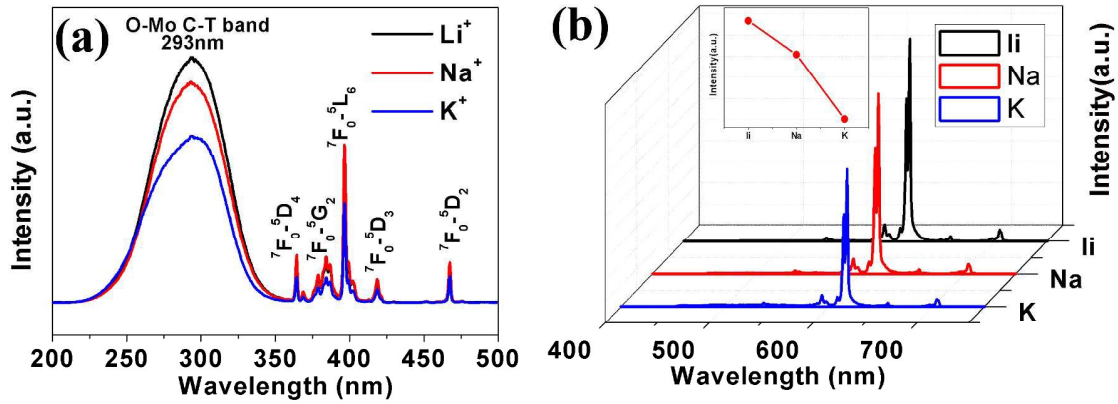

Figure 20. (a) Excitation and (b) Emission spectra of $CaMoO_4$: Eu^{3+}, M^+ with different charge compensator phosphors

The photoluminescence properties of the as-prepared $CaMoO_4:Eu^{3+}$, M^+ with different charge compensator phosphors were investigated at room temperature.

As shown in Figure 20,the shape and positions are the same in the excitation spectra and emission spectra for $CaMoO_4:Eu^{3+}$, M^+ (M =Li，Na，K) samples . However, it can be seen that Li^+, Na^+ or K^+ ions have different influences on the luminescent intensity. The red emission peak intensity of $CaMoO_4:Eu^{3+}$ using Li^+ and Na^+ ions as charge compensator is higher than that of K^+ ions, Li^+ ions have the best charge compensation effect. Because K^+ ion (0.138nm) has the largest ionic radius, which is larger than that of Ca^{2+} (0.100), Na^+ (0.102nm) and Li^+ (0.076nm), and hence it is relatively difficult to substitute Ca^{2+} with K^+ in the crystal lattice of $CaMoO_4$, which in turn leads to the lowest luminescence intensity.

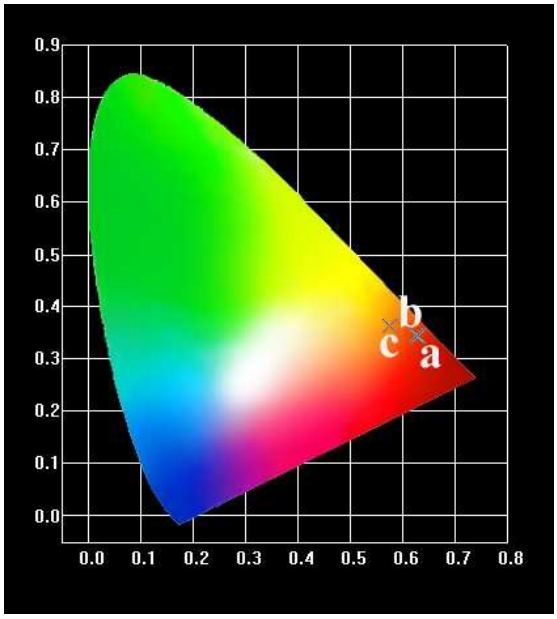

Figure 21. CIE color coordinates of $CaMoO_4:Eu^{3+}$, M^+ with different charge compensator microspheres phosphors (a) $CaMoO_4:Eu^{3+}$, Li^+, (b) $CaMoO_4:Eu^{3+}$, Na^+, (c) $CaMoO_4:Eu^{3+}$, K^+.

Figure 21 showed the CIE chromaticity coordinates of $CaMoO_4:Eu^{3+}$, M^+ (M=Li，Na，K) based on their corresponding emission spectra. The CIE color coordinate of the $CaMoO_4:Eu^{3+}$, Li^+, $CaMoO_4:Eu^{3+}$, Na^+, $CaMoO_4:Eu^{3+}$, K^+ microspheres phosphor is (0.63, 0.34), (0.62, 0.35), (0.57, 0.36), respectively. They are close to the standard of NTSC (x = 0.67, y = 0.33), indicating that $CaMoO_4$: Eu^{3+}, M^+ (M=Li，Na，K) microspheres phosphors have a good

color purity and potential application for red phosphors.

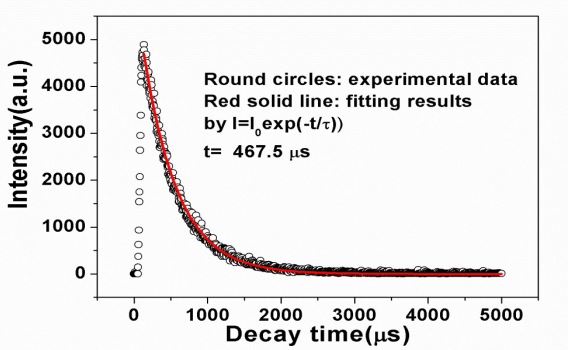

Figure 22. The PL decay curves for the as-synthesized $CaMoO_4:Eu^{3+}$, Na^+ microspheres samples

The PL decay curves for the as-synthesized $CaMoO_4:Eu^{3+}$, Na^+ microspheres samples were also studied. Figure 22 showed the decay curves for the $^5D_0$–$^7F_2$ transition of Eu^{3+} in $CaMoO_4:Eu^{3+}$, Na^+, which can all be well fitted into a single exponential function as $I = I_0 \exp(-t/\tau)$, where τ is the decay lifetime, I_0 is the initial intensity and t is decay time. The lifetime is determined to be 467.5μs for $^5D_0$–$^7F_2$ emission of Eu^{3+}.

4. Conclusions

A facile PDDA-modulated coprecipitation hydrothermal route was used to synthesize high-quality and monodisperse $CaMoO_4:Eu^{3+}$, M^+（M =Li，Na，K）microspheres. The PDDA plays a critical role in the morphology of the final products. Furthermore, the shape and size of the products can be manipulated by adjusting the concentration of PDDA and pH values in the initial solution. The prepared microspheres morphology is stable at the suitable annealing temperature. PL spectra of $CaMoO_4:Eu^{3+}$, Na^+ show that the photoluminescence properties could be improved through different pH and PDDA concentration and hydrothermal treatment and annealing treatment. The particle size and shape have a remarkably effect on the photoluminescence properties of the phosphor. The luminescence intensity is remarkable enhanced

with the increase of annealing temperature due to eliminating PDDA and/or H_2O present in the samples and to the improved crystal quality. The red emission peak intensity of $CaMoO_4:Eu^{3+}$ using Li^+ and Na^+ ions as charge compensator is higher than that of K^+ ions, and Li^+ ions have the best charge compensation effect.

Acknowledgments

This research was supported by the Basic Science Research Program through the National Research Foundation of Korea (NRF) funded by the Ministry of Education, Science and Technology (no. 2010-0029634). The "$CaMoO_4:Eu^{3+}$, M^+（M =Li，Na，K）microspheres" was supplied by the Display and Lighting Phosphor Bank at Pukyong National University. Our study also was supported by the National Natural Science Foundations of China (Grant no. 21301053) and the Natural Science Fund for Creative Research Groups of Hubei Province of China (No. 2014CFA015).

References

1. A. P. Alivisatos, *Science*, 1996, **271**, 933-937.
2. J. Hu, T. W. Odom and C. M. Lieber, *Acc. Chem. Res.*, 1999, **32**, 435-445.
3. Y. Xia, Y. Xiong, B. Lim and S. E. Skrabalak, *Angew. Chem. Int. Ed.*, 2009, **48**, 60-103.
4. S. Gai, C. Li, P. Yang and J. Lin, *Chem. Rev.*, 2014, **114**, 2343-23 89.
5. G. Blasse and B. C. Grabmaier, eds., *Luminescent Materials*, Springer Berlin, 1994.
6. A. M. Kaczmarek and R. Van Deun, *Chem. Soc. Rev.*, 2013, **42**, 8 835-8848.
7. J. C. Sczancoski, M. D. R. Bomio, L. S. Cavalcante, M. R. Joya, P. S. Pizani, J. A. Varela, E. Longo, M. S. Li and J. A. Andrés, *J. Phys. Chem. C*, 2009, **113**, 5812-5822.
8. N. Sharma, K. M. Shaju, G. V. Subba Rao, B. V. R. Chowdari, Z. L. Dong and T. J. White, *Chem. Mater*, 2003, **16**, 504-512.
9. F. A. Rabuffetti, S. P. Culver, L. Suescun and R. L. Brutchey, *Ino*

rg. Chem., 2014, **53**, 1056-1061.
10. Q. Gong, X. Qian, H. Cao, W. Du, X. Ma and M. Mo, *J. Phys. Chem. B*, 2006, **110**, 19295-19299.
11. C. Hazra, T. Samanta, A. V. Asaithambi and V. Mahalingam, *Dalto n. Trans.*, 2014, **43**, 6623-6630.
12. B. P. Singh, A. K. Parchur, R. S. Ningthoujam, A. A. Ansari, P. S ingh and S. B. Rai, *Dalton. Trans.*, 2014, **43**, 4779-4789.
13. B. P. Singh, A. K. Parchur, R. S. Ningthoujam, A. A. Ansari, P. S ingh and S. B. Rai, *Dalton. Trans.*, 2014, **43**, 4770-4778.
14. S. Yan, J. Zhang, X. Zhang, S. Lu, X. Ren, Z. Nie and X. Wang, *J. Phys. Chem. C*, 2007, **111**, 13256-13260.
15. Y. Hu, W. Zhuang, H. Ye, D. Wang, S. Zhang and X. Huang, *J. Alloys Compd.*, 2005, **390**, 226-229.
16. S. Yu, Z. Lin, L. Zhang and G. Wang, *Crystal Growth & Design*, 2007, **7**, 2397-2399.
17. A. K. Parchur, R. S. Ningthoujam, S. B. Rai, G. S. Okram, R. A. Singh, M. Tyagi, S. C. Gadkari, R. Tewari and R. K. Vatsa, *Dalto n. Trans.*, **40**, 7595-7601.
18. Y. Yang, X. Li, W. Feng, W. Yang, W. Li and C. Tao, *J. Alloys Compd.*, 2011, **509**, 845-848.
19. G. S. R. Raju, E. Pavitra, Y. H. Ko and J. S. Yu, *J. Mater. Che m.*, 2012, **22**, 15562-15569.
20. A. Xie, X. Yuan, S. Hai, J. Wang, F. Wang and L. Li, *J. Phys. D: Appl. Phys.*, 2009, **42**, 105107.
21. Z. H. Zhang, Q. Huang, X. Zhao and Z. L. Huang, *Phys. Status. Solidi. A*, 2009, **206**, 2839-2843.
22. J. Liu, H. Lian and C. Shi, *Opt. Mater.*, 2007, **29**, 1591-1594.
23. G.h. Peng, X. Wang, Z.h. Liang, Y.c. Wang, X.b. Han and J.l. Wu, *J. Alloys Compd.*, 2013, **576**, 227-231.
24. Y.S. Luo, X.J. Dai, W.D. Zhang, Y. Yang, C. Q. Sun and S.Y. Fu, *Dalton. Trans.*, 2010, **39**, 2226-2231.
25. V. S. Marques, L. S. Cavalcante, J. C. Sczancoski, A. F. P. Alcânt ara, M. O. Orlandi, E. Moraes, E. Longo, J. A. Varela, M. Siu Li and M. R. M. C. Santos, *Crystal Growth & Design*, 2010, **10**, 475 2-4768.
26. Z. Hou, R. Chai, M. Zhang, C. Zhang, P. Chong, Z. Xu, G. Li an d J. Lin, *Langmuir*, 2009, **25**, 12340-12348.
27. Y. Jin, J. Zhang, S. Lu, H. Zhao, X. Zhang and X.j. Wang, *J. Phy s. Chem. C*, 2008, **112**, 5860-5864.
28. V. M. Longo, L. c. S. Cavalcante, E. C. Paris, J. l. C. Sczancoski, P. S. Pizani, M. S. Li, E. Longo and J. A. Varela, *J. Phys. Chem. C*, 2011, **115**, 5207-5219.

29. Q. Gong, X. Qian, X. Ma and Z. Zhu, *Crystal Growth & Design*, 2006, **6**, 1821-1825.
30. F. Yu, J. Zuo, Z. Zhao, C. Jiang and Q. Yang, *Mater. Res. Bull.*, 2011, **46**, 1327-1332.
31. T. Thongtem, S. Kungwankunakorn, B. Kuntalue, A. Phuruangrat an d S. Thongtem, *J. Alloys Compd.*, 2010, **506**, 475-481.
32. C. Xu, D. Zou, H. Guo, F. Jie and T. Ying, *J. Lumin.*, 2009, **129**, 474-477.
33. Y.J. Zhu and F. Chen, *Chem. Rev.*, 2014, **114**, 6462-6555.
34. Y. Sun, C. Li, Z. Zhang, X. Ma, L. Wang, Y. Wang, M. Song, P. Ma, L. Jiang and Y. Guo, *Solid State Sc.*, 2012, **14**, 219-224.
35. D. Chen, K. Tang, F. Li and H. Zheng, *Crystal Growth & Design*, 2005, **6**, 247-252.
36. Q. Zhang and Z. Xia, *RSC Adv.*, 2014, **4**, 53237-53244.
37. X. Bao, S. Zhou, J. Wang, L. Zhang, S. Huang and Y. Pan, *Mater. Res. Bull.*, 2013, **48**, 1034-1039.
38. W. X. H. Y. P. G. L. Z. W. JL, *Chin. J. Mater. Res*, 2012, **26**, 6 15-620.
39. M.J. Kim and Y.D. Huh, *Opt. Mater.*, 2012, **35**, 263-267.
40. Y. Zhou, J. Liu, X. Yang, X. Yu and L. Wang, *J. Electrochem. Soc.*, 2011, **158**, K74-K80.
41. G. Wakefield, E. Holland, P. J. Dobson and J. L. Hutchison, *Adv. Mater.*, 2001, **13**, 1557-1560.
42. J.G. Li, X. Li, X. Sun and T. Ishigaki, *J. Phys. Chem. C*, 2008, **1 12**, 11707-11716.
43. Y. Wang, S. Gai, C. Li, X. Zhang, N. Niu, F. He, M. Zhang and P. Yang, *RSC Adv.*, **3**, 5945-5955.
44. T. Wang, H. Colfen and M. Antonietti, *J. Am. Chem. Soc.*, 2005, **1 27**, 3246-3247.
45. V. Dmitrovic, G. J. M. Habraken, M. M. R. M. Hendrix, W. J. E. M. Habraken, A. Heise, G. de With and N. A. J. M. Sommerdijk, *Polymers*, 2012, **4**, 1195-1210.
46. S. Liu, S. Tian and R. Xing, *CrystEngComm*, 2011, **13**, 7258-7261.
47. S. P. Culver, F. A. Rabuffetti, S. Zhou, M. Mecklenburg, Y. Song, B. C. Melot and R. L. Brutchey, *Chem. Mater.*, 2013, **25**, 4129-4 134.
48. M. P. Ghaderi, JM; Campbell, IH; Sylvester, PJ, *J. Econ. Geol. Bu ll. Soc.*, 1999, **94**, 423-437.
49. S. H. Yu, B. Liu, M. S. Mo, J. H. Huang, X. M. Liu and Y. T. Qian, *Adv. Funct. Mater.*, 2003, **13**, 639-647.
50. B. Liu, S.H. Yu, L. Li, Q. Zhang, F. Zhang and K. Jiang, *Angew. Chem. Int. Ed.*, 2004, **43**, 4745-4750.

51. Z. Fu, W. Xia, Q. Li, X. Cui and W. Li, *CrystEngComm*, 2013, **14**, 4618-4624.
52. F. Han, Z. Guan, T. S. Tan and Q.H. Xu, *ACS Applied Materials & Interfaces*, 2012, **4**, 4746-4751.
53. L. Du, S. Zhang, G. Chen, G. Yin, C. Du, Q. Tan, Y. Sun, Y. Qu and Y. Gao, *ACS Applied Materials & Interfaces*, 2014, **6**, 14043-14049.
54. D. Alloyeau, C. Ricolleau, C. Mottet, T. Oikawa, C. Langlois, Y. Le Bouar, N. Braidy and A. Loiseau, *Nat Mater*, 2009, **8**, 940-946.
55. D. Gebauer, A. Volkel and H. Colfen, *Science*, 2008, **322**, 1819-1822.
56. B. Fleury, M.A. Neouze, J.M. Guigner, N. Menguy, O. Spalla, T. Gacoin and D. Carriere, *ACS Nano*, 2014, **8**, 2602-2608.
57. A. Dey, P. H. H. Bomans, F. A. Muller, J. Will, P. M. Frederik, G. de With and N. A. J. M. Sommerdijk, *Nat Mater*, 2010, **9**, 1010-1014.
58. X. Liu, L. Li, H. M. Noh, B. K. Moon, B. C. Choi and J. H. Jeong, *Dalton. Trans.*, 2014, **43**, 8814-8825.
59. A. F. Kirby and F. S. Richardson, *J. Phys. Chem.*, 1983, **87**, 2544-2556.
60. J. W. Stouwdam and F. C. J. M. van Veggel, *Nano Lett.*, 2002, **2**, 733-737.
61. G. Blasse and A. Bril, *J. Inorg. Nucl. Chem.*, 1967, **29**, 2231-2241.
62. J. Huang, J. Xu, H. Luo, X. Yu and Y. Li, *Inorg. Chem.*, 2011, **50**, 11487-11492.
63. A. K. Singh, S. K. Singh and S. B. Rai, *RSC Adv.*, 2014, **4**, 27039-27061.
64. D. Chen, G. Shen, K. Tang, Z. Liang and H. Zheng, *J. Phys. Chem. B*, 2004, **108**, 11280-11284.
65. G. Blasse, *Prog. Solid State Chem.*, 1988, **18**, 79-171.
66. A. Huignard, T. Gacoin and J.P. Boilot, *Chem. Mater.*, 2000, **12**, 1090-1094.